

Perturbation impact of spectators and spurious qubit interactions on a cross-resonance gate in a tunable coupling superconducting circuit

Tianqi Cai,^{1,*} Xiyue Han,^{1,*} Yukai Wu,¹ Yulin Ma,¹ Jiahui Wang,¹
Hongyi Zhang,¹ Haiyan Wang,¹ Yipu Song,^{1,†} and Luming Duan^{1,‡}

¹*Center for Quantum Information, Institute for Interdisciplinary Information Sciences, Tsinghua University, Beijing 100084, China*

Cross-resonance (CR) gate has proved to be a promising scheme for implementing fault-tolerant quantum computation with fixed-frequency qubits. In this work, we experimentally implement an entangling cross-resonance gate by using a microwave-only control in a tunable coupling superconducting circuit. The flux-controlled tunable coupler allows us to continuously vary adjacent qubit coupling from positive to negative values, and thus providing an extra degree of freedom to verify optimal condition for constructing the CR gate. Based on three-qubit CR Hamiltonian tomography, we systematically investigate the dependency of gate fidelities on spurious interaction components and present the first experimental approach to evaluate the perturbation impact arising from the spectator qubits. Our results reveal that the spectator qubits can lead to reductions in the CR gate fidelity relying on the particular frequency resonance poles and the induced ZZ interaction between the spectator and gate qubits, while an improvement in the gate fidelity to 98.5% can be achieved by optimally tuning the inter-qubit detuning and flux bias on the coupler. Our experiments uncover an optimal CR operation regime and provide a guiding principle to improve the CR gate fidelity by suppression of unwanted qubit interactions.

I. INTRODUCTION

As enormous progress in superconducting quantum processors has been made towards more complex networks of qubits, it becomes increasingly crucial to develop robust protocols for multi-qubit control [1–4]. In complex superconducting circuits with larger numbers of qubits, the fidelity of quantum algorithms begins to be dominated by unwanted qubit interactions, increased decoherence, and frequency-crowding, all inherent to traditional frequency-tuned architectures [5]. Alternatively, a microwave-only control scheme can provide frequency-selectivity and allows to use fixed-frequency computational qubits, thereby minimizing the sensitivity of the qubits with respect to the sources of possible noise [6, 7]. Cross-resonance (CR) gate is an entangling gate for fixed-frequency qubits by using only microwave control. To perform a CR gate, a microwave drive is applied on a control qubit at the frequency of a target qubit [8]. The gate relies on an always-on coupling between the two qubits, yet it can be turned on and off in principle only via a single microwave drive. Moreover, the gate itself obtains a Clifford group operator $[ZX]^{1/2}$, which is locally equivalent to a universal gate CNOT by only one additional local rotation of each qubit, ie, $\text{CNOT} = [ZI]^{1/2}[ZX]^{1/2}[IX]^{1/2}$ [9, 10]. Consequently, the CR gate scheme has a strong appeal to the multi-qubit control in superconducting architectures using fixed-frequency transmon qubits, thus allowing the qubits to be operated at their optimal bias points for coherence; also, it only requires a single microwave drive line for applying the drive tone to the control qubit and, thereby efficiently reduces the circuit complexity.

The Cross-resonance gate has been demonstrated, obtaining a quantum process tomography (QPT) gate fidelity of 81%, by using a single microwave tone to turn on the CR interaction [8]. The gate process has been improved via a calibration procedure that accurately measures a full CR Hamiltonian, achieving an interleaved randomized benchmarking fi-

delity over 99% [11]. A fast two-qubit gate relies on a large coupling, but leading to crosstalk between qubits. Accordingly, the CR implementation is hindered by the trade-off between a short gate time and high gate fidelity. Recent study has revealed that, besides the cross resonance component ZX , the CR drive Hamiltonian also involves unwanted qubit interactions, for instance, IX, IY, IZ, ZZ term, etc [11]. As this intractability emerges, to eliminate the unwanted terms, it becomes crucial to investigate the dependency of the unwanted components on the variation of the coupling between qubits. However, this has not yet been previously explored due to a less control of the interactions between qubits. Up to date, experimental realization of tunable couplers provides a way to adjust qubit interactions, hence offers a possibility for mitigating unwanted couplings [12–14]. Meanwhile, CR gate has been used in small-scale multi-qubit demonstrations of fault-tolerant protocols [1, 15]. In practice, however, computational qubits of CR gate will not be isolated from environment and are always connected to neighboring qubits in a quantum processor [16, 17]. In particular, a recent theoretic study on CR gate reveals detrimental multi-qubit frequency collisions as a control or target qubit couples to a third spectator qubit [18], and yet it remains highly desired for an experimental investigation of optimal CR gate operation in the presence of spectator qubit.

In this paper, we address these crucial barriers to optimizing CR gate control, by systematically investigating the dependency of gate fidelities on spurious interaction components. This study presents the first experimental approach to evaluate the perturbation impact arising from the spectator qubits, providing a guiding principle to improve the CR gate fidelity by suppression of the qubit-spectator interactions. Our experimental results reveal that the spectator qubits have a significant impact on the computational gate qubits, leading to reduction in the gate fidelity dependent on the specific frequency of spectator qubits and the induced ZZ interaction with

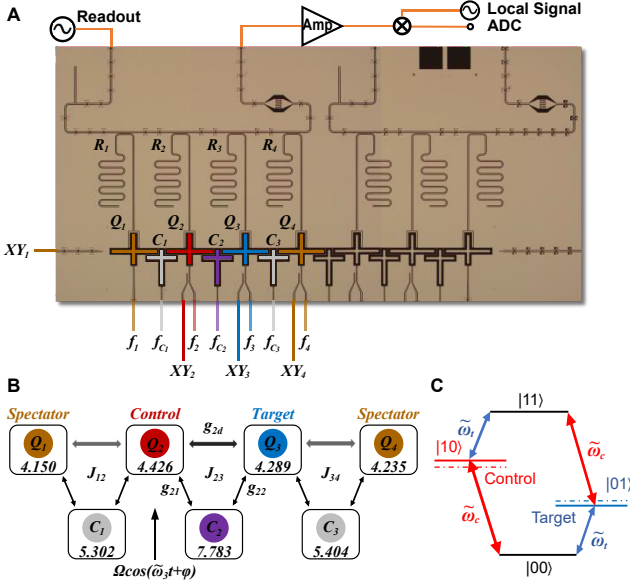


FIG. 1. (A) Optical micrograph of thirteen Xmon qubits with the bottom six qubits serving as tunable couplers. Each computational qubit on both sides of the couplers has independent XY and Z control, and is coupled to a separate $\lambda/4$ resonator for simultaneous and individual readout. The couplers each have an individual flux-bias line for frequency tunability. The combination of direct capacitive coupling and indirect tunable coupling via the coupler constitutes the total coupling between the two adjacent computational qubits. The colored part represents the subsystem used in the experiment. (B) Sketch of the coupler system used in experiment which has one-to-one correspondence with the colored part in (A). The red, blue and yellow qubits represent the control, target, and spectator qubits respectively. The qubit frequencies are shown in the box. The two computational qubits are coupled with an effective coupling J_{23} via a direct coupling with strength g_{2d} and indirect couplings through the coupler with g_{21} and g_{22} , respectively. (C) Energy spectrum of a pair of weakly coupled qubits as J_{23} is small compared to $\Delta(\phi)$. Dashed (solid) lines depict uncoupled (coupled) energy levels for Q_2 (red, labeled as control) and Q_3 (blue, labeled as target).

the gate qubits. By optimally tuning the inter-qubit detuning and flux bias on the coupler, we achieve a CR gate fidelity of 98.5%, primarily limited by qubit decoherence.

II. RESULTS

A. Isolated Cross-resonance Gate

Our quantum processor consists of seven transmon qubits ($Q_i, i = 1 \sim 7$) with each pair of neighboring qubits mediated via a frequency-tunable coupler ($C_j, j = 1 \sim 6$), as shown in Fig. 1(A). Each tunable coupler has a symmetric Josephson junction with a cross-shaped capacitor sandwiched between the two neighboring qubits, contributing to the total coupling between the two computational qubits. Each qubit, Q_i and C_j , has a dedicated flux bias line to tune its frequency by threading the magnetic flux through the transmon junction loop. In our

experiments, the qubits, $Q_i (i = 2, 3)$ and $Q_i (i = 1, 4)$ as outlined in Fig. 1(B), are used to implement the CR gate as the computational gate qubits and spectator qubits, respectively.

The two gate qubits $Q_i (i = 2, 3)$ each couple to the tunable coupler C_2 with a coupling strength g_{21}, g_{22} , as well as to each other with a direct capacitive coupling strength g_{2d} . Both qubits are negatively detuned from the coupler, $\Delta_i(\phi) = \omega_i - \omega_c < 0 (i = 2, 3)$, where $\omega_{2,3}$, ω_c are the frequencies of Q_2 , Q_3 and C_2 . The experimentally extracted parameters, $g_{21}, g_{22}/2\pi = 63$ MHz, $g_{2d}/2\pi \sim 5.5$ MHz, give a dispersive coupling, $g_{21}, g_{22} \ll |\Delta_i(\phi)|$ (see Supplementary Material [19] for details). We apply a cross-resonance (CR) drive pulse on the control qubit Q_2 , $\Omega \cos(\omega_{dt} + \phi)$, with an amplitude Ω , frequency ω_d and phase ϕ . When the qubit drive is present, the system Hamiltonian states as,

$$H/\hbar = \sum_{i=2,3} \frac{1}{2} \tilde{\omega}_i \sigma_i^z + J_{23} (\sigma_2^+ \sigma_3^- + \sigma_3^+ \sigma_2^-) + \Omega \cos(\omega_{dt} + \phi) \sigma_2^x \quad (1)$$

where σ_α^x , σ_α^z , σ_α^+ , σ_α^- ($\alpha = 2, 3$) are the Pauli X, Pauli Z, raising and lowering operators for Q_2 and Q_3 respectively; $\tilde{\omega}_2 = \omega_2 + \frac{J_{23}}{\Delta(\phi)}$, $\tilde{\omega}_3 = \omega_3 - \frac{J_{23}}{\Delta(\phi)}$, $J_{23} = g_{2d} + \frac{g_{21}g_{22}}{\Delta(\phi)}$, $\frac{1}{\Delta(\phi)} = (\frac{1}{\Delta_2(\phi)} + \frac{1}{\Delta_3(\phi)})/2$ [20–22]. The combination of two terms, $g_{2d} + \frac{g_{21}g_{22}}{\Delta(\phi)}$, gives the total effective qubit-qubit coupling J_{23} , which can be adjusted by the coupler frequency through $\Delta(\phi)$. Energy spectrum shown in Fig. 1(C) depicts the corresponding qubit frequency shift as J_{23} is small compared to $\Delta(\phi)$. Since the tunability is continuous, one can always find a critical value to turn off the effective coupling J_{23} , as well as the static ZZ coupling [13]. On the condition that $\Omega, J_{23} \ll \Delta(\phi)$, and the drive frequency ω_d is in resonance with the target qubit (Q_3) frequency $\tilde{\omega}_3$, under the consideration of crosstalks on the chip and off-resonance drive on the control qubit, the effective drive Hamiltonian can be expressed as $H_{eff}/\hbar = u_1 ZX + u_2 ZY + u_3 ZZ + u_4 ZI + u_5 IX + u_6 IY + u_7 IZ$ [11, 23]. The first one is the cross-resonance (CR) term, while the rests are the unwanted residual qubit interaction terms in the gate operation. For instance, the forth term represents an ac-Stark shift due to the off-resonance drive on the control qubit, and the fifth one reflects the crosstalk on the target qubit. Based on energy-basis representation method, in consideration of both the higher-level effects of the qubits and classical crosstalks, the CR term can be calculated as $u_1 = J_{23} \Omega (1 - A_c) \left(\frac{v_{3,01} v_{2,12}^2}{\Delta_{23} + \alpha_2} - \frac{2v_{3,01} v_{2,01}^2}{\Delta_{23}} \right)$ [18], where A_c denotes the suppression in the drive tone on the control qubit, $v_{i,01}, v_{i,12} (i = 2, 3)$ are dimensionless extracted parameters which are defined in Supplementary Materials [19], α_2 is anharmonicity of Q_2 , $\Delta_{23} = \tilde{\omega}_2 - \tilde{\omega}_3$.

To verify optimal implementation parameters and determine specific error terms in the gate operation, we experimentally measured the CR Hamiltonian to distinguish the various drive Hamiltonian components, as a function of the control-target qubit frequency detuning and the flux bias on the coupler. Following the approach developed in the report [11], we similarly fit the set of Rabi oscillations with a

Bloch equation model function. The CR drive Hamiltonian can then be derived in terms of the six possible interactions IX, IY, IZ, ZX, ZY, ZZ . As varying the frequency detuning, coupler flux bias and the CR drive amplitude, we perform the CR Hamiltonian tomography using a previously implemented method. The corresponding pulse sequence used for the measurement is depicted in Supplementary Materials [19]. We plot the measured ZX and ZZ interaction in Fig. 2(A),(B) as a function of the control-target frequency detuning $\Delta_{ct} = \Delta_{23}$ at eight different flux biases on the coupler with a fixed CR drive amplitude $\Omega = 18$ MHz. Solid lines represent the numerical calculation results based on the lowest-order energy-basis representation method [18]. A cross-sectional view of Fig. 2(A),(B) by choosing two representative coupler frequencies is illustrated in Fig. 2(C) and (D), with a variation of CR drive amplitudes. The results reveal that the interaction components are sensitive to the frequency detuning Δ_{23} , featuring two-qubit resonance poles as the detuning crosses the gate parameters $\Delta_{23} = 0, \Delta_{23} = \pm\alpha_i = \pm222$ MHz ($i = 2, 3$), and thus divide the gate operation into three distinct regions labeled with I, II and III, see Fig. 2(C). Besides, the primary interaction components ZX, ZZ and IX are plotted in Fig. 2(E) as varying the drive amplitude and the DC flux bias on the coupler with fixed $\Delta_{ct} = 152$ MHz. With the increase of the DC flux bias, the coupler qubit frequency is reduced to be close to the gate qubit frequency. Consequently, the CR ZX interaction slowly varies from positive to negative but turns to a rapid change as the coupler frequency goes below a turning point around 4.6 GHz for each drive amplitude, demonstrating a tunability range of about $5.6 \sim -3.9$ MHz (experimental data) with $\Omega = 31$ MHz as an example. The ZZ term shows a relatively smaller variation range, keeping positive interaction but increasing rapidly below the turning point. The IX interaction, however, monotonically decreases from about -34.9 to -22.5 MHz (experimental data) with $\Omega = 31$ MHz, showing a much stronger dependence on the CR drive amplitude. We find that the large ZX rate while relatively small static ZZ interaction in region III defines an optimal operating regime in our experiment, which is confirmed by the experimental data and numerical calculations (solid lines) shown in the top panel of Fig. 2(F). In addition, the bottom panel of Fig. 2(F) implies that ZX/ZZ is less sensitive to the coupler frequency except for the region near $ZZ = 0$.

To suppress the unwanted CR components, we verify an appropriate CR drive phase at which the ZX component is maximized while the ZY is zero by measuring the CR Hamiltonian parameters as a function of the drive phase, as shown in Supplementary Materials [19]. To further eliminate the cross-talk term IX and other unwanted interactions ZZ and ZI , we perform the CR Rabi experiment using an echo scheme to re-focus these terms [11]. The echo sequence involves a π pulse and a change of sign of the CR drive on the control qubit, as depicted in Fig. 3(A). Clearly, in Fig. 3(B), the echo scheme indeed improves the CR Rabi oscillations on the target qubit, which are much closer to sinusoidal oscillations expected for a ZX drive compared to the one obtained by using the pulse

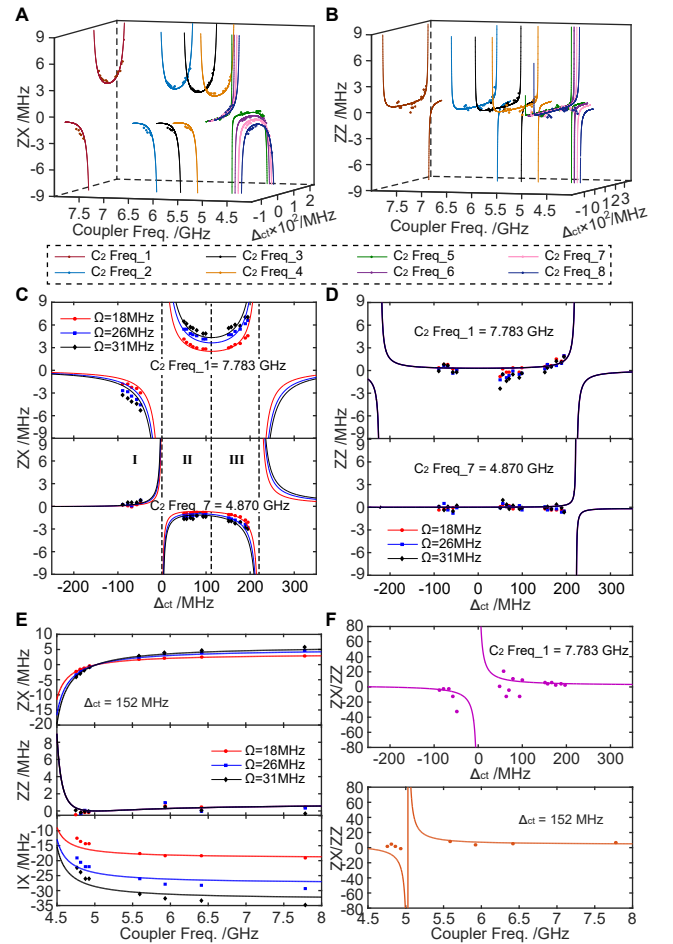


FIG. 2. (A)(B) The ZX and ZZ interactions extracted from CR Hamiltonian tomography (dots) vary with the control-target frequency detuning Δ_{ct} and coupler frequency. The CR drive amplitude is fixed at $\Omega = 18$ MHz. The numerical calculations (solid lines) based on the lowest-order energy-basis representation method fit well with the experimental results(dots). (C)(D) Cross-sectional views of (A)(B) with two specific coupler frequencies. The three sets of data present the ZX and ZZ interactions with respect to the CR drive amplitude of 18, 26 and 31 MHz, respectively. The large ZX rate while small ZZ interaction in region III defines the optimal operating regime for the CR gate. (E) The variation of primary interaction components ZX, ZZ and IX as a function of the coupler frequency in a range of $4.5 \sim 8.0$ GHz (calculation data) with three different CR drive amplitudes. (F) The experimental (dots) and numerical (solid lines) results of ZX/ZZ ratio varying with the qubit frequency detuning Δ_{ct} (top panel) and the coupler frequency (bottom panel). The optimal operating condition is expected in the region where the ZX/ZZ ratio is large but insensitive to the coupler frequency.

sequence without echo integration. The R vector plotted in the figure is the norm distance between Bloch vectors of the target qubit corresponding to the control qubit in $|0\rangle$ and $|1\rangle$, which can be defined as $\|\vec{R}\| = \sqrt{\sum_{r=x,y,z} (\langle r_0 \rangle + \langle r_1 \rangle)^2}$. The two qubits are maximally entangled when R vector goes to zero, hence we can use $\|R\|$ to estimate the gate length for perform-

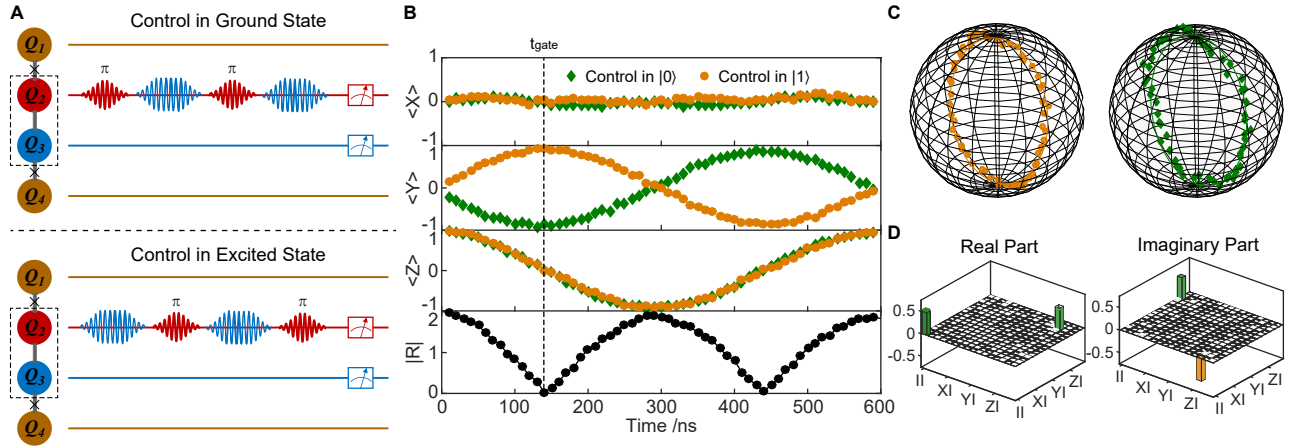


FIG. 3. (A) Echoed pulse sequence involves a π pulse and a change of sign of the CR drive on the control qubit. (B) CRabi oscillations on the target qubit projected onto x , y , and z for the control in $|0\rangle$ and $|1\rangle$. Sinusoidal oscillations are expected for a ZX drive. R vector, $R = 0$ indicates the gate time of maximal entanglement. (C) Trajectory of the target qubit state on the Bloch sphere during the echoed CR gate evolution. For the control in $|0\rangle$ (left column) and $|1\rangle$ (right column). A perfect ZX gate would result in a circle on the surface of the Bloch sphere. (D) Measured QPT result for an entangling CR gate with a gate length of 220 ns (CR pulse: 140 ns; two single-qubit π pulses: 40 ns for each). The solid black outlines are for the ideal gate.

ing the entangling gate, which is about 140 ns as marked in Fig. 3(C). Apparently, the result shows a full contrast of $\langle y \rangle$ while non-oscillation of $\langle x \rangle$, indicating that the IY term has been cancelled out. As illustrated in Fig. 3(C), the trajectory of the target qubit depicted in a Bloch sphere during the CR gate operation, showing a near perfect circle on the surface of the Bloch sphere, further confirms that the echo scheme improves the gate evolution.

The ratio of the desired ZX term to the unwanted ZZ component uncovers optimal detuning spots to achieve low coherent error for the CR gate. According to the results shown in Fig. 2(F), we finally choose $\Delta_{ct} = 137$ MHz with the coupler (C_2) frequency of 7.783 MHz to be the optimal operating position where one expects to yield a high gate fidelity and low two-qubit coherent error. Indeed, we verify the CR gate fidelity as varying the inter-qubit detuning and DC flux bias on the coupler. We perform quantum process tomography (QPT) for the CR gate by implementing 16 independent two-qubit input states and construct the Pauli transfer matrix χ . The gate fidelity can be determined from the χ matrix through the expression $F = \text{tr}(\chi_{\text{exp}}\chi_{\text{ideal}})$, where χ_{exp} and χ_{ideal} are the experimental and ideal χ matrix. Fig. 3(D) shows the χ_{exp} and χ_{ideal} for a CR entangling gate acquired under the optimal condition. The gate fidelity from QPT is 98.5% from maximum-likelihood estimation, primarily limited by qubit decoherence [24].

B. Cross-resonance Gate with Spectator Qubits

Since the physical coupling with surrounding qubits inevitably exists in multi-qubit system, the dispersive coupling between gate qubits and spectator qubits will undoubtedly af-

fect the gate fidelity. In order to explore a more realistic scenario of gate operation, we conduct CR gate with considering a third spectator qubit which could be coupled to either the control or the target qubit, see the schematic circuit in Fig. 1(B). Q_1 and Q_4 are treated as control spectator and target spectator, coupling to the control qubit Q_2 and the target qubit Q_3 with an effective coupling strength J_{12} and J_{34} , respectively. Under the consideration of anharmonicity for each qubit, the system can be described by the Hamiltonian $H = H_{\text{gate}} + H_{\text{spec}}$, where:

$$H_{\text{gate}}/\hbar = \sum_{i=2,3} \omega_i a_i^\dagger a_i - \frac{\alpha_i}{2} a_i^\dagger a_i^\dagger a_i a_i + J_{23}(a_2^\dagger a_3 + a_2 a_3^\dagger) + \Omega \cos(\omega_d t + \phi)(a_2 + a_2^\dagger), \quad (2)$$

$$H_{\text{spec}}/\hbar = \sum_{i=1,4} \omega_i a_i^\dagger a_i - \frac{\alpha_i}{2} a_i^\dagger a_i^\dagger a_i a_i + J_{12}(a_1^\dagger a_2 + a_1 a_2^\dagger) + J_{34}(a_3^\dagger a_4 + a_3 a_4^\dagger).$$

where $\omega_i, \alpha_i (i = 1 \sim 4)$ are the frequencies and anharmonicities of each qubit, respectively. H_{gate} generates the effective two-qubit ZX term as discussed above, while H_{spec} represents the potential effects of the spectator qubits acting on the gate qubits. In the dispersive regime, the coupling between gate qubits and spectator qubits results in a parasitic ZZ crosstalk between Q_1 and Q_2 as well as the one between Q_3 and Q_4 . In addition, as the spectator frequency crosses some specific values, unexpected multi-qubit resonances may induce a failure of the CR gate operation [18].

Hamiltonian tomography is a useful tool for distinguishing various interaction components and determining specific error terms in gate operation. Nevertheless, when considering a larger network of qubits, the original Hamiltonian parameters should be modified to account for the impact of spectator

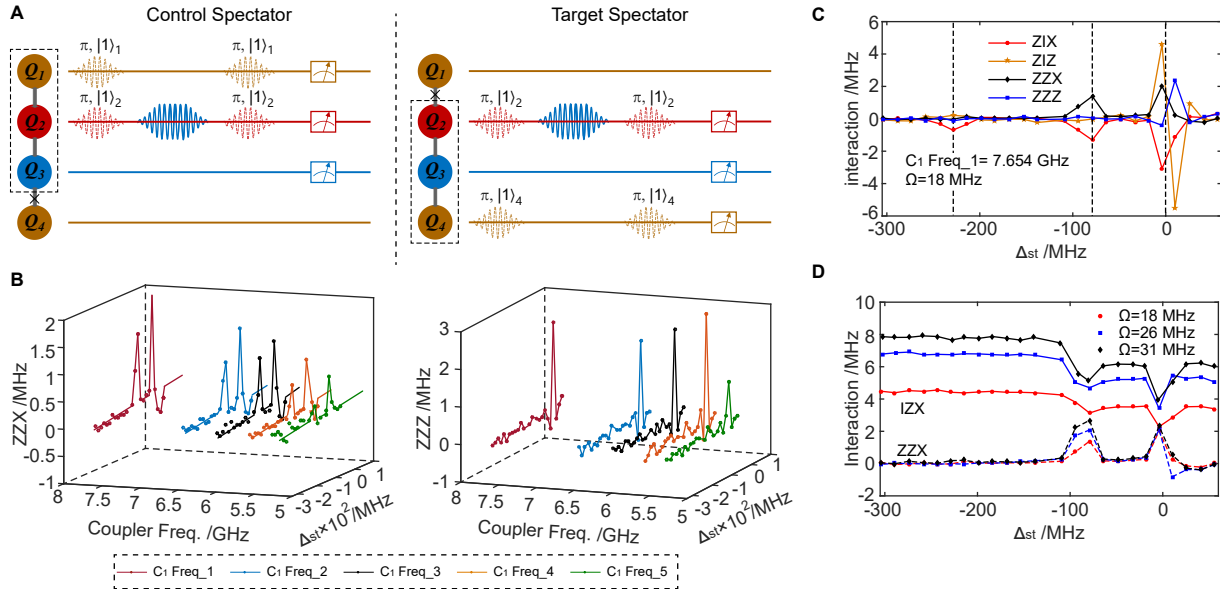


FIG. 4. (A) The schematic pulse sequences for measuring three-qubit Hamiltonian tomography with either a control-spectator qubit (left panel) or a target-spectator qubit (right panel). For the control-spectator case, a CR pulse is applied on the control qubit in the spectator-control subspace of $|00\rangle, |01\rangle, |10\rangle, |11\rangle$, respectively. For example, when measuring Rabi oscillation of the target qubit in the subspace of $|10\rangle$ and $|11\rangle$, two π pulses are consequently applied on Q_1 before and after the CR pulse. Three-qubit simultaneous single-shot readout is then performed to measure the interaction terms based on Eq. (4). Note that the coupling between Q_3 and Q_4 is always closed during the process. Similarly, for the target-spectator case, the CR pulse is applied on the control qubit in the target-spectator subspace with $|00\rangle, |01\rangle, |10\rangle$ and $|11\rangle$ respectively, keeping the coupling between Q_1 and Q_2 closed. (B) The dominant three-qubit CR Hamiltonian ZZX (ZZZ) term in the control-spectator case varying with the change of Δ_{st} (tuning qubit frequency of Q_1) and J_{12} (changing coupler frequency of C_1). (C) The dominant interaction terms, in the control-spectator case, varying as a function of Δ_{st} with a fixed coupler frequency of C_1 at 7.654 GHz (the maximum frequency of C_1) and a CR drive amplitude at 18 MHz. Apparently, all interaction terms demonstrate an extreme change in some specific detuning regions ($\Delta_{st} = 0, -85, -222$ MHz), revealing unwanted energy excitations happened in the CR gate operation. (D) Three-qubit IZX and ZZX terms varying with the Δ_{st} and CR drive amplitude in the control spectator case. The IZX is crucial for implementing CR gate, while the ZZX is the error term generated from the spectator qubit. Clearly, the interaction terms are more sensitive at the specific detuning positions with larger drive amplitude.

qubits. It is obvious that the CR drive pulse is only resonant with the effective target qubit frequency, hence, apart from the target qubit containing all the Pauli interactions $\{I, X, Y, Z\}$ with others, both the control qubit and spectator qubits should only involve $\{I, Z\}$ interactions. Based on these, without loss of generality, we consider a minimal extension of the original isolated CR model and develop an approach for three-qubit CR Hamiltonian tomography with either a control or a target spectator qubit, respectively.

For clarity, the gate operators with a control-spectator qubit is naturally taken as $|\text{spectator}\rangle \otimes |\text{control}\rangle \otimes |\text{target}\rangle = \{I, Z\} \otimes \{I, Z\} \otimes \{I, X, Y, Z\}$. Therefore, the full CR drive Hamiltonian with the control-spectator qubit has a following form:

$$H = \frac{I \otimes I \otimes A}{2} + \frac{I \otimes Z \otimes B}{2} + \frac{Z \otimes I \otimes C}{2} + \frac{Z \otimes Z \otimes D}{2}, \quad (3)$$

where $A, B, C, D \in \{X, Y, Z\}$. We experimentally measure the three-qubit Hamiltonian tomography to extract primary interaction terms. This is accomplished by turning on the CR drive for some time and then measuring the Rabi oscillations on the target qubit in the $\text{spectator} \otimes \text{control}$ subspace

at $|00\rangle, |01\rangle, |10\rangle, |11\rangle$, for projecting the target qubit state onto x , y and z axis. Similar to the approach developed for the two-qubit Hamiltonian tomography, the Rabi oscillations can still be fitted with a Bloch equation model function, $\vec{r}_{\{00,01,10,11\}}(t) = e^{Gt} \vec{r}_{\{00,01,10,11\}}(0)$, ($r = x, y, z$). $\vec{r}(t)$ is the vector composed of the three projecting measurement values, $\langle x(t) \rangle, \langle y(t) \rangle, \langle z(t) \rangle$, as a function of the length of the Rabi drive. G is a matrix defined as

$$\begin{pmatrix} 0 & \Delta^{\{00,01,10,11\}} & \Omega_y^{\{00,01,10,11\}} \\ -\Delta^{\{00,01,10,11\}} & 0 & -\Omega_x^{\{00,01,10,11\}} \\ -\Omega_y^{\{00,01,10,11\}} & -\Omega_x^{\{00,01,10,11\}} & 0 \end{pmatrix} \quad (4)$$

where $\Delta^{\{00,01,10,11\}}$ is the control drive detuning, and $\Omega_{x,y}^{\{00,01,10,11\}}$ is the Rabi drive amplitude of the x, y component, in respect of the $\text{spectator} \otimes \text{control}$ subspace in $|00\rangle, |01\rangle, |10\rangle, |11\rangle$. Accordingly, all the interaction terms in Eq. (3) can be easily acquired. For example, $IZX = (\Omega_x^{00} - \Omega_x^{01} + \Omega_x^{10} - \Omega_x^{11})/8$, $ZZX = (\Omega_x^{00} - \Omega_x^{01} - \Omega_x^{10} + \Omega_x^{11})/8$ [19].

The dominant effects of spectator qubits can be manifested in two aspects: the frequency shift of gate qubit due to ZZ interaction with spectator qubits and the specific frequency

detuning regions involving two- or three-qubit resonances. Therefore, to further explore these effects, we separately extract the three-qubit CR drive Hamiltonian terms with changing the coupling strength J_{12} between Q_1 and Q_2 and the frequency detuning Δ_{st} between Q_1 and Q_3 . The schematic pulse sequence is outlined in the left panel of Fig. 4(A). Here, we fix the gate qubits Q_2 and Q_3 at the optimal gate position, with $\Delta_{23} = 137$ MHz, according to the isolated two-qubit CR Hamiltonian tomography shown in Fig. 2. The coupler C_2 is biased at 7.783 GHz, offering a positive coupling between the gate qubits.

We vary Δ_{st} and J_{12} by changing the frequency of the spectator qubit Q_1 and the coupler C_1 , respectively. Fig. 4(B) shows the dominant three-qubit gate parameters, ZZX and ZZZ , extracted from the Bloch equation Eq. (4) as a function of Δ_{st} and J_{12} . A further cross-sectional view in Fig. 4(C) illustrates more primary interaction terms. Apparently, for certain resonance regions, unwanted energy excitations appear, breaking down the CR gate regime. For instance, the condition of $\Delta_{st} = 0$ leads to a resonance of $|100\rangle$ and $|001\rangle$, while the parameters in the region around $\Delta_{st} = -85$ MHz result in a resonance of $|110\rangle$ and $|020\rangle$. Except for these regions, the interaction terms remain almost intact with different coupling strengths. Moreover, the interaction terms like ZIX , ZZX , ZIZ , ZZZ describe the effective mediated interaction between the control-spectator Q_1 and the target qubit Q_3 through the control qubit Q_2 . These terms undoubtedly affect the evolution of the target qubit, and thus degrade the CR gate fidelity. Consequently, we choose an appropriate frequency of control-spectator qubit Q_1 so that the detuning Δ_{st} is tuned away from the resonance poles. Furthermore, these three-qubit Hamiltonian interaction terms also have a dependence on the CR drive amplitude. As an example, the ZZX and IZX interactions illustrated in the right panel of Fig. 4(D), enhance with the increase of CR drive amplitude, in particular, more pronounced in the resonance pole region for the ZZX term.

Similar to the case with the control-spectator qubit, the gate operators with a target-spectator qubit can be correspondingly taken as $|control\rangle \otimes |target\rangle \otimes |spectator\rangle = \{I, Z\} \otimes \{I, X, Y, Z\} \otimes \{I, Z\}$. Then, the CR drive Hamiltonian with the target-spectator qubit can be expressed as:

$$H = \frac{I \otimes A \otimes I}{2} + \frac{Z \otimes B \otimes I}{2} + \frac{I \otimes C \otimes Z}{2} + \frac{Z \otimes D \otimes Z}{2}, \quad (5)$$

Naturally, based on the Bloch equation Eq. (4), we can conduct three-qubit CR Hamiltonian tomography with a target-spectator qubit as varying the spectator-target detuning Δ_{st} , frequency of coupler C_3 and CR drive amplitude. A similar pulse sequence is depicted in the right panel of Fig. 4(A). Compared with the perturbation impact of the control-spectator qubit, we find that the target-spectator qubit seems to affect the CR gate operation more seriously as Δ_{st} is close to resonance poles inducing unwanted energy transfer. In fact, this can be understood that a slight jitter of the target qubit frequency either from the static ZZ interaction between Q_3 and Q_4 or the unwanted energy resonance at $\Delta_{st} = 0$ be-

tween $|001\rangle$ and $|010\rangle$ as an example, will seriously disturb or even break down the CR gate operation where the target qubit undertakes the main evolution process while the control qubit is not directly excited. The detailed dependency of the interaction terms on the Δ_{st} , J_{34} and CR drive amplitude in the target-spectator case can be found in Supplementary Materials [19].

III. DISCUSSIONS

So far, we have analyzed the underlying physical mechanisms and characterized the three-qubit CR Hamiltonian tomography in detail under the consideration of a control-spectator qubit or a target-spectator qubit. For both situations, we find that unwanted energy level resonances are the leading factors for breaking down the gate evolution, and meanwhile, the increase of CR drive amplitude will enhance all the interactions including the error terms. In this section, we take a step further to explore the perturbation impact of spectator qubits on the CR gate fidelity. The outcomes demonstrate that the qubit frequencies and coupling strength between the qubits should be carefully chosen to reach a balance between high CR gate fidelity and feasibility of gate operation, in particular in a large superconducting network, where one qubit could be treated as a gate qubit in one network block but practically behaves as a spectator qubit in another.

We now explore the dependency of CR gate fidelity on the coupling strength between the spectator qubits and gate qubits. We extract ZZ interaction between the spectator and gate qubit and measure QPT gate fidelity as varying the coupling strength by modifying the frequencies of C_1 and C_3 . The parameters of Q_2 , Q_3 and C_2 are chosen according to the optimal condition for isolated two-qubit CR gate operation, while the frequencies of spectator qubits, Q_1 and Q_4 , are tuned to the appropriate positions based on the three-qubit Hamiltonian tomography shown in Fig. 4, avoiding potential resonance poles which break down the gate operation.

We first extract the ZZ interaction, between Q_1 and Q_2 , Q_3 and Q_4 , via a Ramsey-type experiment which involves probing the frequency of one qubit with another in either its ground or excited state [25, 26]. The ZZ interaction occurs as the coupling between the spectator and gate qubit is on, and its magnitude rises as the increase of the coupling strength, as depicted as color bar shown in Fig. 5(B). For comparison of perturbation impact from the spectator qubits in various conditions, we execute multiple sets of QPT experiments for each operation index, selectively applying π or $\pi/2$ pulse on either Q_1 or Q_4 , respectively. The experimentally measured QPT results are shown in Fig. 5(B) and the corresponding pulse sequence is illustrated in Fig. 5(A). The QPT measurement with idle pulse (without pulse) on the spectator qubits (in ground state) sets a control fidelity for each operation index with the particular coupling condition, for comparing with the measurements with pulse applied on the spectator qubits (experimental fidelity). The relative gate error in Fig. 5(B), defined as

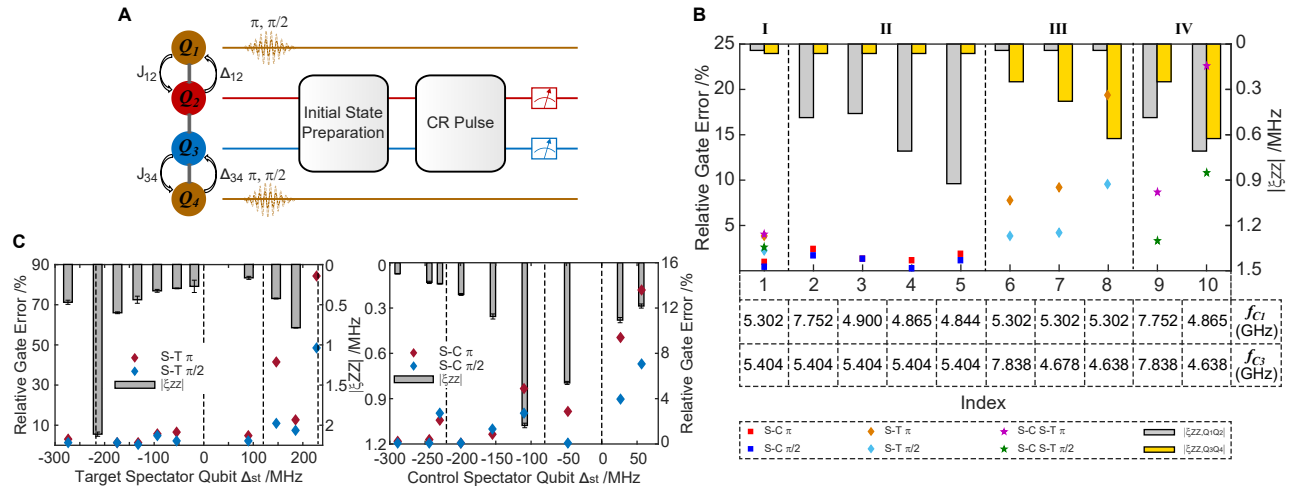


FIG. 5. (A) The schematic pulse sequence for the exploration of CR gate fidelity with spectator qubits. The qubit frequencies of Q_2 , Q_3 and Q_4 are biased at 4.426, 4.289 and 7.783 GHz respectively, and Δ_{23} is fixed at the optimal frequency detuning of 137 MHz throughout the QPT measurements. We categorize the operation into four regions: I: both couplings (J_{12} and J_{34}) off (index 1); II: J_{12} coupling on while J_{34} off (index 2-5); III: J_{12} off while J_{34} on (index 6-8); IV: both J_{12} and J_{34} on (index 9-10). For each operation index, multiple sets of QPT experiments containing idle, π or $\pi/2$ pulse on the spectator qubits are used to extract the relative gate error between the control groups and experimental groups. (B) The relative QPT gate error and ZZ interaction vs the coupling strength between the spectator qubits and gate qubits. The colored points display the different pulse sequences applied to the spectator qubits. For example, the red-square point represents a π pulse applied on the control-spectator qubit Q_1 before the QPT experiment on the gate qubits. The gray and yellow bars show the ZZ interaction between Q_1 and Q_2 , Q_3 and Q_4 , respectively. The qubit frequencies of Q_1 and Q_4 are tuned at 4.150 and 4.235 GHz, respectively. (C) The relative QPT gate error and ZZ interaction vs the frequency detuning of the spectator Q_1 and Q_4 to the target qubit Q_3 , respectively. The CR gate fidelity is affected not only by the ZZ interaction between the gate qubits and spectator qubits, but also by the unwanted energy excitations in the specific frequency resonance pole regions. The frequency position labeled with dotted line refers to the resonance poles which may lead to a failure in the CR gate.

the difference between the experimental fidelity and the control fidelity, reflexes the perturbation impact from the spectator qubits on the CR gate, because of the factor that once the spectator qubit is excited, the ZZ interaction between the spectator and gate qubit will disturb the CR gate evolution, thus degrading the gate fidelity. As expected, the spectator qubits have almost no perturbation impact on the gate qubit regardless of the operations of the spectator qubits, as the couplings between the gate qubits and spectator qubits are turned off (see index region I). Once the coupling is on, however, the perturbation impact obviously occurs, and the relative gate error increases as the magnitude of ZZ interaction (between the spectator and gate qubits) rises. Particularly, the gate qubits are more susceptible to the perturbation impact from the target-spectator qubit (index region III) than that from the control-spectator qubit (index region II). The perturbation impact becomes more serious, evidenced by the larger relative gate error, when both the couplings between Q_1/Q_2 and Q_3/Q_4 are all on (index region IV).

We further characterize the dependency of CR gate fidelity on the frequency detuning of the spectator Q_1 and Q_4 to the target qubit Q_3 , exploring the impact factors due to both the ZZ interactions and unwanted energy excitations. Fig. 5(C) shows the relative gate error and ZZ interaction as varying the frequency detuning in the control-spectator case (right panel) and target-spectator case (left panel), respectively. In

the control-spectator case, the frequency of Q_1 is changed, while biasing the frequency of C_1 at 7.752 GHz (yield the maximum positive coupling between Q_1 and Q_2) and keeping off the interaction between Q_3 and Q_4 (via tuning the coupler frequency C_3 or adjusting the qubit frequency of Q_4 far away from the gate qubits). In a similar way, the frequency of Q_4 is varied for the target-spectator case, while tuning the frequency of C_3 at 7.838 GHz (reach the maximum positive coupling between Q_3 and Q_4). Corresponding to the particular resonance pole regions as shown in Fig. 4 and Supplementary Materials [19], we observe that the unwanted energy excitations play a major role in degrading the CR gate fidelity, showing larger relative-gate errors in general at the resonance poles compared to that at other detuning positions even with stronger ZZ interactions. Whereas, the relative gate error relies more on the ZZ interactions at the other detuning positions without resonance poles.

IV. CONCLUSIONS

In summary, we employ the flux-controlled tunable coupler to verify the optimal operation condition for constructing the CR gate and provide a guiding principle to improve the CR gate fidelity in large-scale quantum circuits. We here emphasize our main conclusions: (1) We present the first experimen-

tal approach to evaluate the perturbation impact arising from the spectator qubits. The perturbation impact is enhanced on the particular resonance poles where unwanted energy excitations are induced, and the target-spectator qubit leads to more serious degrading of the CR gate fidelity than the control-spectator qubit. (2) We systematically investigate the dependency of gate fidelities on spurious interaction components by tuning the inter-qubit detuning and flux bias on the coupler. The interaction terms rely on the coupling strength and frequency detuning between the spectator and gate qubits, and the CR drive amplitude. The dominant interaction terms are more pronounced in the resonance pole regions. (3) The three-qubit Hamiltonian tomography method we develop here can be extended and applied to other multibody systems to extract multi-qubit Hamiltonian interaction terms. Our experimental outcomes will be highly desirable as the CR gate implementation becomes more widely used in large scale superconducting circuits and fault-tolerant quantum computation.

ACKNOWLEDGMENTS

We acknowledge Luyan Sun for sharing JPA fabrication parameters. This work was supported by the National Natural Science Foundation of China under Grant No.11874235, the State's Key Project of Research and Development Plan under Grant No. 2016YFA0301902 and the Tsinghua University Initiative Scientific Research Program.

phase gate for superconducting qubits," *New Journal of Physics* **15**, 115012 (2013).

- [8] J. M. Chow, A. D. Córcoles, J. M. Gambetta, C. Rigetti, B. R. Johnson, J. A. Smolin, J. R. Rozen, G. A. Keefe, M. B. Rothwell, M. B. Ketchen, and M. Steffen, "Simple all-microwave entangling gate for fixed-frequency superconducting qubits," *Physical Review Letters* **107**, 080502 (2011).
- [9] C. Rigetti and M. Devoret, "Fully microwave-tunable universal gates in superconducting qubits with linear couplings and fixed transition frequencies," *Physical Review B* **81**, 134507 (2010).
- [10] J. C. Pommerening, "Multiqubit coupling dynamics and the cross-resonance gate," (2017).
- [11] S. Sheldon, E. Magesan, J. M. Chow, and J. M. Gambetta, "Procedure for systematically tuning up cross-talk in the cross-resonance gate," *Physical Review A* **93**, 060302 (2016).
- [12] P. Mundada, G. Zhang, T. Hazard, and A. Houck, "Suppression of qubit crosstalk in a tunable coupling superconducting circuit," *Physical Review Applied* **12** (2019), 10.1103/physreappplied.12.054023.
- [13] X. Li, T. Cai, H. Yan, Z. Wang, X. Pan, Y. Ma, W. Cai, J. Han, Z. Hua, X. Han, Y. Wu, H. Zhang, H. Wang, Y. Song, L. Duan, and L. Sun, "Tunable coupler for realizing a controlled-phase gate with dynamically decoupled regime in a superconducting circuit," *Physical Review Applied* **14**, 024070 (2020).
- [14] X. Y. Han, T. Q. Cai, X. G. Li, Y. K. Wu, Y. W. Ma, Y. L. Ma, J. H. Wang, H. Y. Zhang, Y. P. Song, and L. M. Duan, "Error analysis in suppression of unwanted qubit interactions for a parametric gate in a tunable superconducting circuit," *Physical Review A* **102**, 022619 (2020).
- [15] A. Córcoles, E. Magesan, S. J. Srinivasan, A. W. Cross, M. Steffen, J. M. Gambetta, and J. M. Chow, "Demonstration of a quantum error detection code using a square lattice of four superconducting qubits," *Nature Communications* **6** (2015), 10.1038/ncomms7979.
- [16] F. Arute, K. Arya, R. Babbush, D. Bacon, J. C. Bardin, R. Barends, R. Biswas, S. Boixo, F. G. S. L. Brandao, and e. a. David A. Buell, "Quantum supremacy using a programmable superconducting processor," *Nature* **574**, 505 (2019).
- [17] M. S. Blok, V. V. Ramasesh, T. Schuster, K. O'Brien, J. M. Kreikebaum, D. Dahmen, A. Morvan, B. Yoshida, N. Y. Yao, and I. Siddiqi, "Quantum information scrambling in a superconducting qutrit processor," *arXiv preprint arXiv:2003.03307* (2020).
- [18] M. Malekakhlagh, E. Magesan, and D. C. McKay, "First-principles analysis of cross-resonance gate operation," *Physical Review A* **102**, 042605 (2020).
- [19] Supplementary materials.
- [20] A. Blais, J. Gambetta, A. Wallraff, D. I. Schuster, S. M. Girvin, M. H. Devoret, and R. J. Schoelkopf, "Quantum-information processing with circuit quantum electrodynamics," *Physical Review A* **75**, 032329 (2007).
- [21] S. Bravyi, D. P. DiVincenzo, and D. Loss, "Schrieffer-wolff transformation for quantum many-body systems," *Annals of Physics* **326**, 2793 (2011).
- [22] F. Yan, P. Krantz, Y. Sung, M. Kjaergaard, D. L. Campbell, T. P. Orlando, S. Gustavsson, and W. D. Oliver, "Tunable coupling scheme for implementing high-fidelity two-qubit gates," *Physical Review Applied* **10**, 054062 (2018).
- [23] E. Magesan and J. M. Gambetta, "Effective hamiltonian models of the cross-resonance gate," *Physical Review A* **101**, 052308 (2020).
- [24] A. N. Korotkov, "Error matrices in quantum process tomography," *arXiv preprint arXiv:1309.6405* (2013).

* These two authors contributed equally to this work.

† ypsong@mail.tsinghua.edu.cn

‡ lmduan@tsinghua.edu.cn

- [1] J. M. Gambetta, J. M. Chow, and M. Steffen, "Building logical qubits in a superconducting quantum computing system," *npj Quantum Information* **3** (2017), 10.1038/s41534-016-0004-0.
- [2] C. Song, K. Xu, H. Li, Y.-R. Zhang, X. Zhang, W. Liu, Q. Guo, Z. Wang, W. Ren, J. Hao, *et al.*, "Generation of multicomponent atomic schrödinger cat states of up to 20 qubits," *Science* **365**, 574 (2019).
- [3] A. A. Houck, H. E. TĂŒreci, and J. Koch, "On-chip quantum simulation with superconducting circuits," *Nature Physics* **8**, 292 (2012).
- [4] C. Neill, P. Roushan, K. Kechedzhi, S. Boixo, S. V. Isakov, V. N. Smelyanskiy, A. Megrant, B. Chiaro, A. Dunsworth, K. Arya, *et al.*, "A blueprint for demonstrating quantum supremacy with superconducting qubits," *Science* **360**, 195 (2018).
- [5] R. A. Pinto, A. N. Korotkov, M. R. Geller, V. S. Shumeiko, and J. M. Martinis, "Analysis of a tunable coupler for superconducting phase qubits," *Physical Review B* **82**, 104522 (2010).
- [6] S. Poletto, J. M. Gambetta, S. T. Merkel, J. A. Smolin, J. M. Chow, A. D. Córcoles, G. A. Keefe, M. B. Rothwell, J. R. Rozen, D. W. Abraham, C. Rigetti, and M. Steffen, "Entanglement of two superconducting qubits in a waveguide cavity via monochromatic two-photon excitation," *Physical Review Letters* **109**, 240505 (2012).
- [7] J. M. Chow, J. M. Gambetta, A. W. Cross, S. T. Merkel, C. Rigetti, and M. Steffen, "Microwave-activated conditional-

- [25] M. Reed, “Entanglement and quantum error correction with superconducting qubits,” (2013).
- [26] J. M. Chow, “Quantum information processing with superconducting qubits,” (2010).